Kinetic effects in a Hall thruster discharge[a)]

I. D. Kaganovich[b)] and Y. Raitses
Plasma Physics Laboratory, Princeton University, Princeton, New Jersey 08543

D. Sydorenko[c)] and A. Smolyakov
University of Saskatchewan, Saskatoon, SK, S7H3E6, Canada

(Received 31 October 2006; accepted 24 January 2007; published online 1 May 2007)

Recent analytical studies and particle-in-cell simulations suggested that the electron velocity distribution function in $E \times B$ discharge of annular geometry Hall thrusters is non-Maxwellian and anisotropic. The average kinetic energy of electron motion in the direction parallel to the thruster channel walls (across the magnetic field) is several times larger than that in the direction normal to the walls. Electrons are stratified into several groups depending on their origin (e.g., plasma or channel walls) and confinement (e.g., lost on the walls or trapped in the plasma). Practical analytical formulas are derived for the plasma flux to the wall, secondary electron fluxes, plasma potential, and electron cross-field conductivity. Calculations based on these formulas fairly agree with the results of numerical simulations. The self-consistent analysis demonstrates that the elastic electron scattering in collisions with atoms and ions plays a key role in formation of the electron velocity distribution function and the plasma potential with respect to the walls. It is shown that the secondary electron emission from the walls may significantly enhance the electron conductivity across the magnetic field but only weakly affects the insulating properties of the near-wall sheath. Such self-consistent decoupling between the secondary electron emission effects on the electron energy losses and the electron cross-field transport is currently not captured by the existing fluid and hybrid models of Hall thrusters. © *2007 American Institute of Physics*. [DOI: 10.1063/1.2709865]

I. INTRODUCTION

There is reliable experimental evidence of the wall material effect on operation of a Hall thruster.[1,2] Figure 1 shows the dependence of the electron temperature on discharge voltage for different wall materials. The existing fluid theories explain this effect invoking a strong secondary electron emission (SEE) from the channel walls. The SEE is predicted to weaken insulating properties of the near-wall sheaths and, thereby (i) to cause cooling of plasma electrons and (ii) to enhance the electron conductivity across the magnetic field. From a practical standpoint, a strong SEE from the channel walls is expected to cause additional inefficiencies due to enhanced power losses in the thruster discharge and intense heating of the channel walls by almost thermal electron fluxes from the plasma.[3] Moreover, because the SEE leads to lower values of the sheath potential drop, ion-induced erosion of the channel walls can be also affected. Although these predictions can be certainly applied for plasmas with a Maxwellian electron velocity distribution function (EVDF), there is no consensus between the existing fluid[2,4–7] and kinetic models[8,9] on how strong the SEE effects on the thruster plasma are. According to kinetic simulations,[8–12] the EVDF in a collisionless plasma is depleted at high energies due to electron-wall losses. Under such conditions, the electron losses to the walls can be hundreds of times smaller than the losses predicted by the fluid theories. A similar depletion of EVDF at high energies was also reported for other kinds of low-pressure gas discharges.[13–15] Note that the deviation of the EVDF from a Maxwellian does not necessarily mean that the SEE cannot play a significant role in the thruster discharge. In experiments with a Hall thruster operating at high discharge voltages, the maximum electron temperature and the electron cross-field current were strongly affected by the SEE properties of the channel wall materials, as shown in Fig. 1 (Refs. 16 and 17).

In recent particle-in-cell (PIC) simulations[10–12] and in the kinetic study,[13] we showed that the SEE effect on power losses in a thruster discharge is quite different from what was predicted by previous fluid and kinetic studies. In simulations, the EVDF was found to be strongly anisotropic, depleted at high energies, and in some cases, even nonmonotonic. The average kinetic energy of electron motion in the direction parallel to the walls is several times larger than the average kinetic energy of electron motion in the direction normal to the walls. Secondary electrons form two beams propagating between the walls of a thruster channel in opposite radial directions[10,11] (also predicted in Ref. 18 in the modified fluid approximation). In the present paper, the focus is on the role of the elastic electron scattering (due to electron-atom and Coulomb collisions) in the formation of the EVDF and, consequently, on its role in the electron-wall interaction processes in the thruster discharge. It is shown that for a typical high-performance Hall thruster, the electron fluxes to the walls are limited by the source of electrons, overcoming the wall potential and leaving the plasma. The flux of these electrons is determined mainly by the frequencies of elastic electron collisions with atoms and ions. The sheath insulating properties depend on the electron fluxes to

[a)]Paper QI2 5, Bull. Am. Phys. Soc. **51**, 222 (2006).
[b)]Invited speaker.
[c)]Present address: University of Alberta, Edmonton, AB, T6G 2G7, Canada.

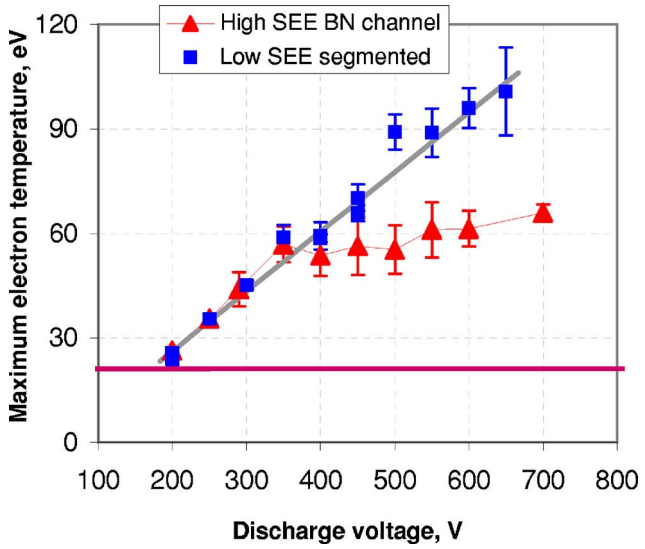

FIG. 1. (Color online) The dependence of the maximum electron temperature on the discharge voltage for the conventional thruster with high-SEE boron nitride channel walls and the segmented thruster with low-SEE floating segmented electrodes made of carbon velvet material from Ref. 17. The horizontal (magenta) line shows the fluid theory predictions.

the walls and, therefore, on the rate of elastic scattering of plasma electrons.

In previous kinetic studies, Meezan and Cappelli[8] developed a kinetic model based on the so-called nonlocal approach. The nonlocal approach (described, for example, in Ref. 19) was developed for large gas discharges with the distance between walls (gap) of order tens of centimeters and at pressures above 10 mTorr, where the electron mean free path is much smaller than the discharge gap $\lambda_c \ll H$. Because of the smallness of the electron mean free path in these gas discharges, the EVDF is isotropic even for electrons with energy high enough to overcome the wall potential. In Hall thrusters the characteristic distance between walls is given by the channel width. The traditional nonlocal approach is not applicable to Hall thrusters, which operate in the opposite limit $\lambda_c \gg H$. Because the electron mean free path in Hall thrusters is much larger than the channel width, the EVDF has been shown to be anisotropic.[11] Moreover, the anisotropy of the EVDF strongly affects the electron flux to the wall, as shown below. Practical analytical formulas are derived for wall fluxes, secondary electron fluxes, plasma parameters, and contribution to the electron current due to SEE. The calculations based on the analytical formulas agree well with the results of numerical simulations.

An important implication of the present work is that future theoretical and experimental studies need to determine the influence of these kinetic effects on the thruster performance, heating, and erosion of the channel walls. For instance, the reduction of the gas density in the thruster channel might significantly reduce the electron fluxes to the walls because in xenon plasmas of Hall thrusters the electron collisions with neutral atoms is the major scattering process while the Coulomb scattering of the ions gives a small contribution.

II. ELECTRON VELOCITY DISTRIBUTION FUNCTION IN THE HALL THRUSTER CHANNEL

Formation of the EVDF in the channel of a Hall thruster discharge was studied using a one–dimensional particle-in-cell code. Let us discuss applicability of the one-dimensional approach for the EVDF calculations. According to the measurements reported in Refs. 16 and 20 the maximum electron temperature can be a factor of 10 smaller than the discharge voltage (Fig. 1). This means that electrons acquire energy from the electric field and lose it due to inelastic collisions and wall losses many times, while they move from the cathode to the anode. This means that the energy relaxation length is much smaller than the channel width. There are a number of processes resulting in the electron energy loss: inelastic collisions with atoms and ions, losses to the walls, collective interaction between high-energy and low-energy electrons, etc. A typical value for the electron gyroradius, ρ_c, is about a millimeter in the acceleration zone. Plasma electrons can move across the magnetic field lines due to collisions with neutrals or due to turbulent collisions, with the total effective scattering frequency ν_{scat}, leading to a cross-field displacement due to diffusion $x \sim 2\sqrt{D_\perp t}$, where the diffusion coefficient is $D_\perp = \nu_{\text{scat}} \rho_c^2/2$. An electron loses its energy due to inelastic collisions and wall losses with the effective loss frequency ν_{loss} (see Sec. VI for detailed description of ν_{loss}). The energy relaxation length is determined by the distance on which a typical electron traverses during time ν_{loss}^{-1}. This distance is of order $2\rho_c\sqrt{\nu_{\text{scat}}/2\nu_{\text{loss}}}$.

Hybrid simulations of Hall thrusters[21,22] predict neutral gas density of order 10^{12}–10^{13} cm^{-3} in the acceleration region. For the plasma regimes studied in the present work (neutral density of few 10^{12} cm^{-3}), the ratio $(\nu_{\text{scat}}/\nu_{\text{loss}})$ of the effective scattering and loss frequencies is not very high: a factor of a few. Therefore, the energy relaxation length is a few gyroradii, i.e., much smaller than the length of the ion acceleration region (a few centimeters) measured in typical Hall thrusters.[8,20,23–27] Therefore, it follows that the electron kinetics can be essentially described by a one-dimensional model, assuming the values of electric and magnetic field as local parameters. This assumption implies that the electric field and plasma parameters do not change significantly on the scale of energy relaxation length.

Note that it is rather difficult to estimate the exact energy relaxation length in a Hall thruster, because the actual gas density profile is not well known. Therefore, the above assumption of a moderate frequency ratio needs to be verified, probably for each specific Hall thruster. Nevertheless, because of a reasonable neutral density range used in this work, it is believed that the qualitative conclusions described by our one-dimensional model remain valid for two-dimensional (2D) calculations as well.

The code, geometry, and numerical results are described in detail elsewhere.[10–12] In short, we simulate a one-dimensional slab of plasma between emitting walls. Externally applied electric field, E_z, is directed parallel to walls in the z direction; externally applied magnetic field, B_x, is normal to the walls in the x direction. Both are assumed constant. The particle-in-cell code simulates nonuniform plasma

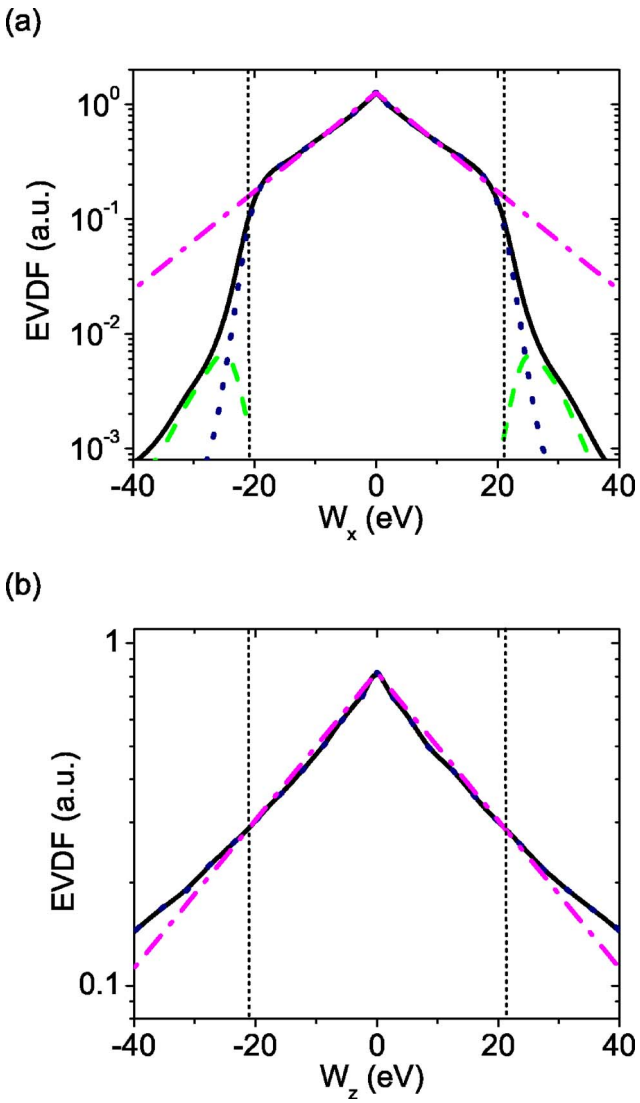

FIG. 2. (Color online) (a) EVDF over the x velocity (normal to the walls) plotted as a function of energy w_x. (Solid black line) total EVDF; (dotted blue line) bulk electrons; (dashed green line) SEE beams; (dot-dashed magenta line) Maxwellian EVDF with T_x=10.1 eV. (b) EVDF over the x velocity (parallel to the walls) plotted as a function of w_z. (Solid black line) bulk EVDF; (dot-dashed magenta line) Maxwellian EVDF with T_z =20.1 eV. EVDFs are obtained in the discharge center; the dashed vertical lines indicate the plasma potential. Plasma parameters correspond to case 1 of Table I.

density profile, sheath, wall fluxes, and EVDF. Typical results of numerical simulations are shown in Figs. 2 and 3. In Fig. 2, the results of the code are shown for E_z=52 V/cm, B_x=91 G, the gas density 2×10^{12} cm^{-3}, which corresponds to the average elastic scattering frequency ν_{en}=1.4 $\times10^6$ s^{-1}. To introduce the anomalous transport along the electric field, E_z, we added an effective frequency of turbulent scattering in the plane perpendicular to magnetic field ν_{turb}=7.8$\times10^6$ s^{-1}. In Fig. 3, E_z=200 V/cm, B_x=100 G, the gas density 10^{12} cm^{-3}, $\nu_{en}=\nu_{\text{turb}}$=0.7$\times10^6$ s^{-1}. The EVDFs shown in Figs. 2 and 3 are generally not Maxwellian and consist of two different groups of electrons: the bulk electrons and SEE beams. Yet, for different electron energy ranges, the EVDF may be approximated by an anisotropic Maxwellian EVDF with the corresponding effective tem-

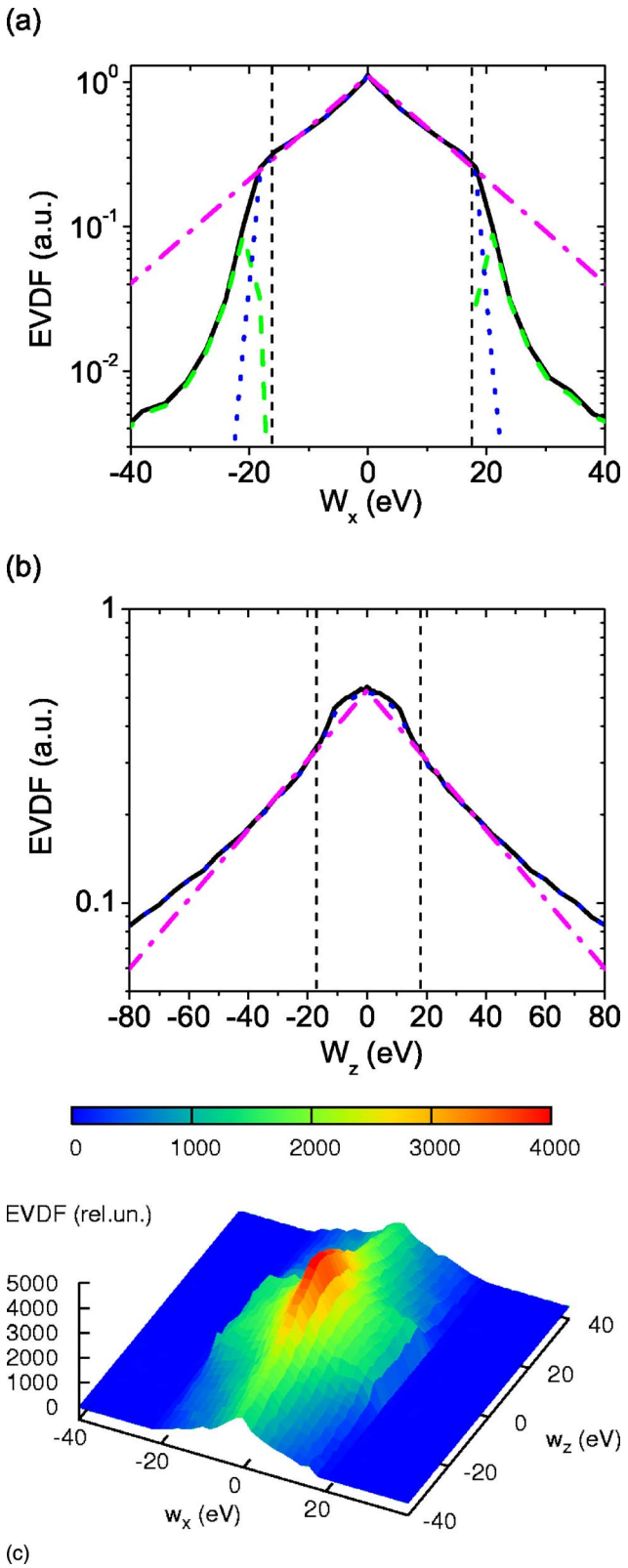

FIG. 3. (Color online) (a) EVDF over the x velocity (normal to the walls) plotted as a function of energy w_x. (Solid black line) total EVDF; (dotted blue line) bulk electrons; (dashed green line) SEE beams; (dot-dashed magenta line) Maxwellian EVDF with T_x=12.1 eV. (b) EVDF over the z velocity (parallel to the walls) plotted as a function of energy w_z. (Solid black line) bulk EVDF; (dot-dashed magenta line) a Maxwellian with T_z =24.1 eV. The dashed vertical lines indicate the plasma potential. (c) The color plot of the two-dimensional EVDF over the x and z velocities plotted as a function of energies w_x and w_z. EVDFs are obtained in the discharge center; the dashed vertical lines in (a) and (b) indicate the plasma potential. Plasma parameters correspond to case 3 of Table I.

TABLE I. Comparison of PIC simulation results with values given by Eqs. (2)–(4), (13), and (15). E_z is the electric field along the plasma channel, parallel to the walls, B_x is the magnetic field in the direction normal to the walls, H is the width of the channel, n_a is the atom density, ν_{turb} is the turbulent collision frequency, Φ is the wall potential, T_{ex} is the electron temperature in the direction normal to the walls obtained by fitting an exponent to $f_x(w_x)$, T_{ez} is the electron temperature in the direction parallel to the walls obtained by fitting an exponent to $f_z(w_z)$, ν_{en} is the average electron-atom elastic scattering collision frequency, λ_c is the electron mean free path corresponding to the electron energy equal to T_{ez}, n_e is the electron density in the discharge center, $\gamma_p = \Gamma_{bp}/\Gamma_{1p}$ is the secondary electron emission coefficient due to the plasma bulk primary electrons only, Γ_{bp} is the flux of secondary electrons emitted from the wall due to the primary flux of plasma bulk electrons Γ_{1p}, $\gamma_b = \Gamma_{bb}/\Gamma_{1b}$ is the secondary electron emission coefficient due to the beam electrons only, Γ_{bb} is the flux of secondary electrons emitted from the wall due to the primary flux of beam electrons coming from the opposite wall Γ_{1b}, J_z is the total electron current, J_{bz} is the electron current due to the contribution of secondary electrons, and $\Gamma_{i,e}$ are the ion and electron flux to the wall from plasma, respectively. $\Gamma_{i,e}$ are in units (10^{20} m^{-2} s^{-1}), f. s. stands for "from simulations," k is the correction coefficient in Eq. (13) $k \equiv T_{ez}^{(\text{for } k=1)}/T_{ez}^{(\text{PIC})}$.

#		Simulation number		1	2	3	4	5	6
1	Simulation parameters (constants) (Refs. 10–12)	SEE included		Yes	No	Yes	No	Yes	No
2		E_z (V/cm)		52	52	200	200	200	200
3		B_x (G)		91	91	100	100	100	100
4		H (cm)		2.5	2.5	2.5	2.5	3	3
5		n_a (10^{12} cm^{-3})		2	2	1	1	1	1
6		ν_{turb} (10^6 s^{-1})		7.81	7.81	0.7	0.7	0.7	0.7
7	Values obtained in simulations	Φ (V)		23	24.1	19.4	25.8	24.9	28
8		T_{ex} (eV)		10.1	10.6	12.1	11.9	12.1	11.9
9		T_{ez} (eV)		20.1	20.4	36.7	41.8	39.3	41.9
10		ν_{en} (10^6 s^{-1})		1.4	1.4	0.7	0.7	0.7	0.7
11		λ_c (m)		1.90	1.91	5.13	5.48	5.31	5.48
12		n_e (10^{11} cm^{-3})		1.93	2.23	1.58	1.70	1.86	1.90
13		γ_p		1.18	n/a	1.59	n/a	1.72	n/a
14		γ_b		0.564	n/a	0.920	n/a	0.732	n/a
15		J_z (A/m^2)		82	89	85	29	45	33
16		J_{bz} (A/m^2)		2.3	n/a	58.4	n/a	13.1	n/a
17		Γ_i (10^{20} m^{-2} s^{-1})		2.44	2.76	2.03	2.23	2.65	2.71
Comparison of simulation results with analytical theory									
18	Estimated parameters	Eq. (3), n_e, T_{ex} f. s.	Γ_i	2.62	3.1	2.35	2.51	2.77	2.80
19		Eq.(2), Φ, T_{ez} f. s.	Γ_e	3.04	3.38	2.3	2.31	2.93	2.89
20		Eq. (4), T_{ex}, T_{ez} f. s.	Φ (V)	25.9	25.8	18.6	21.5	27.1	29.2
21		Eq. (15), Φ, T_{ez} f. s.	T_x (eV)	10.7	11.1	12.7	15.6	15.2	16.8
22		Eq. (13), ν_{en}, ν_{turb}, T_{ex} f. s.	T_z (eV)	28.0	27.7	68.6	68.9	76.8	77.2
23		Correction coefficient	k	1.39	1.36	1.87	1.65	1.96	1.84
24		Eq. (20), $\gamma_{p,b}$, n_e,T_{ex} f. s.	J_{bz} (A/m^2)	3.2	n/a	68.1	n/a	21.5	n/a

peratures, T_{ex} and T_{ez}, shown in Figs. 2 and 3. The EVDF over normal to walls velocity, $f_x(v_x)$, can be obtained by averaging of the three-dimensional (3D) EVDF $f_x(v_x) = \int_{-\infty}^{\infty} dv_y dv_z f(v_x, v_y, v_z)$. This EVDF as a function of $w_x = mv_x^2/2$ incidentally appears to be close to a Maxwellian with an effective "normal" temperature, T_{ex} only for electrons trapped in the potential well, i.e., with the kinetic energy small compared with the potential energy corresponding to the wall potential (the confinement threshold), $w_x < -e\Phi$, as evident in Figs. 2(a) and 3(a). The wall potential is negative relative to the plasma center. However, in the text below, Φ is referred to an absolute value of the wall potential, i.e., without the minus notation.

The EVDF over velocity, in the z direction (parallel to walls) $f_z(v_z)$, can be obtained by averaging of the three-dimensional EVDF $f_z(v_z) = \int_{-\infty}^{\infty} dv_x dv_y f(v_x, v_y, v_z)$. This function, as a function of $w_z = mv_z^2/2$, incidentally appears to be close to a Maxwellian with the effective temperature, T_{ez}, as evident in Figs. 2(b) and 3(b). The exact definitions of these effective temperatures are given in Refs. 11 and 12. Note that due to strong depletion of the EVDF for electron energies above confinement threshold ($w_x > e\Phi$) the ratio between the average temperatures T_{ex} and T_{ez} is an indication of strong anisotropy of the bulk plasma EVDF, in contrast to the ratio of the average energies, $\langle w_x \rangle / \langle w_z \rangle$ (Refs. 10–12), which is an indication of anisotropy of the high-energy part of the EVDF. This is because if the EVDF is a Maxwellian with the same temperatures T_{ex} and T_{ez} in both directions but has a cutoff in the x direction due to wall losses of high-energy electrons with energy $w_x > e\Phi$, the average energy in the z direction is $\langle w_z \rangle = T_{ez}/2$, whereas the average energy in the x direction, $\langle w_x \rangle < T_x/2$ and $\langle w_x \rangle / \langle w_z \rangle < 1$, even though $T_{ex} = T_{ez}$.

Table I summarizes results of numerical simulations for a number of considered thruster cases. Typically, the ratio of the electron temperatures T_{ez}/T_{ex} is about two (compare lines 8 and 9). Note that such a considerable difference between T_{ez} and T_{ex} is highly unusual for the gas discharges. The main reason for this is that the electron mean free path is

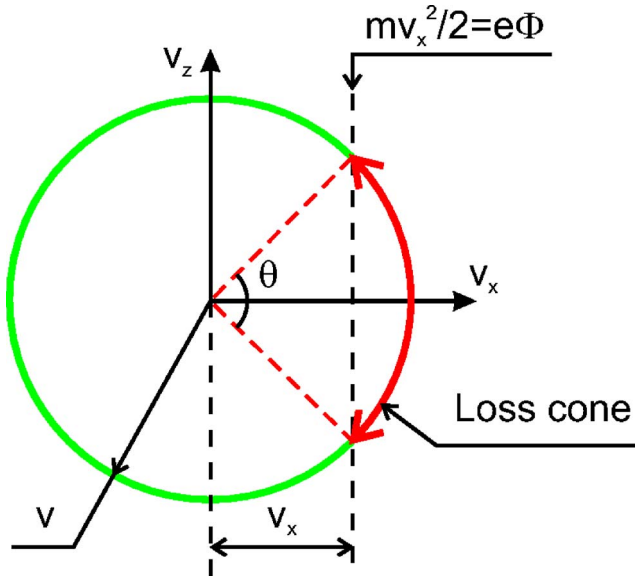

FIG. 4. (Color online) The definition of the loss cone. The cross section of the sphere at $v_y=0$ in the three-dimensional velocity space (v_x,v_y,v_z) for particles with energy $w=m(v_x^2+v_y^2+v_z^2)/2>e\Phi$. The (red) section of the circle marked by arrows is the loss cone.

very large (about 100 cm) as compared to the channel width (~1–3 cm).

It is important to emphasize that according to the results of numerical simulations, the plasma parameters, including the plasma potential and the electron temperatures, are almost insensitive to the SEE. Table I summarizes the results of self-consistent particle-in-cell simulations[10–12] for the same thruster input parameters with and without taking SEE into account. According to these simulations, the SEE strongly increases the electron cross-field current but has little influence on the electron temperature for a given value of the electric field. This result will be discussed in the last section of this paper.

The electrons with energy sufficient to overcome the sheath potential, quickly escape from the plasma to the walls, where depending on their energy, these electrons are either lost due to recombination at the wall or produce secondary electrons. For both events, the high-energy part of the EVDF is strongly depleted [see Figs. 2(a) and 3(a)] and often termed as the loss cone (LC) in the velocity space.[14,15] The loss cone in the velocity space (v_x,v_y,v_z) is shown in Fig. 4. Electrons with a given kinetic energy w form a spherical shell in velocity phase space. If $w>e\Phi$ [where, again, Φ is the plasma potential in the center relative to the wall and $w=m(v_x^2+v_y^2+v_z^2)/2$], then some of these electrons have an energy of motion normal to the wall sufficient to leave the system, $w_x>e\Phi$.

Most of the results in this section are based on analysis of EVDF in an ECR discharge at low pressures developed in Ref. 15 and applied here for the Hall thrusters. The key concept for description of the EVDF and wall losses is the concept of the loss cone. As shown below, the flux to the wall and the effective frequency of electron-wall losses are determined by the loss cone. Therefore, it is important to carefully calculate the loss-cone characteristics. Consider an electron with a total kinetic energy in all directions $w>e\Phi$. In the velocity phase space the velocities of trapped electrons with $w_x<e\Phi$ are located outside the cone with the opening angle, θ such that $\cos(\theta/2)=\sqrt{e\Phi/w}$ (see Fig. 4). Note that the opening angle, θ, depends on the energy w. The total spherical angle of the loss cone in phase space leading to wall losses at one wall is $\Omega_1=2\pi\Omega_1=2\pi\int_0^{\theta/2}\sin\theta' d\theta'=2\pi[1-\cos(\theta/2)]=2\pi[1-e\Phi/w]$. Taking into account two walls gives $\Omega=2\Omega_1$. The EVDF is strongly depleted in the loss cone,[13] as clearly seen in Figs. 2(a) and 3(a). This depletion results in strong reduction of the wall fluxes compared to the case when loss cone is filled.

In the fluid models, it is implicitly assumed that the loss cone is always filled, which is not the case for most collisionless plasmas. Therefore, the conventional fluid expressions for the electron flux to the walls and the sheath potential drop are not applicable for the Hall thruster plasma. The analytical solution of the kinetic equation for the EVDF in the loss cone, f_{lc}, was derived in Ref. 15. The EVDF in the loss cone is filled due to elastic scattering which transfers electrons from outside of the loss cone $(w_x<e\Phi)$ to the loss cone $(w_x>e\Phi)$, and is emptied by a free flight of loss-cone electrons to the walls with a transit time of the order of H/v_x. Here, H is a characteristic size of the plasma bounded between two walls or channel width. In other words, elastic scattering of electrons in the plasma provides a supply of high-energy electrons, which can escape to the walls. Note that the electron distribution function over velocity parallel to the walls (normal to the magnetic field) is not depleted [see Figs. 2(b) and 3(b)]. This is because the main contribution into $f_z(w_z)$ comes from trapped electrons with energy $w_x<e\Phi$, even though $w_z>e\Phi$. The loss rate of these electrons is determined by elastic scattering into the loss cone which is proportional to electron-atom collision frequency, ν_{en}, and is much slower than the loss rate of the energetic electrons with $w_x>e\Phi$, which is given by the transit time estimate $\sim H/v_x$, $\nu_{en}\ll(H/v_x)^{-1}$. In the end, this occurs due to the large electron mean free path, $\lambda_c\gg H$.

In Ref. 15, the solution of the kinetic equation for the EVDF in the loss cone was obtained assuming that the differential cross section has no singularity at small angles. This is correct for an electron kinetic energy of the order of the ionization potential. As discussed above the EVDF outside the loss cone $(w_x<e\Phi)$ is much larger than the EVDF inside the loss cone, where $w_x>e\Phi$. The main processes that form the EVDF inside and outside the loss cone are the elastic scattering and spatial displacement, so that other processes—inelastic collisions and heating—can be neglected. The collisional integral with neutrals can be written in the form: $St(f)=n_a\int(f'-f)v\,d\sigma/d\Omega\,d\Omega$, where n_a is the gas density and f' is the EVDF of electrons before scattering to a given velocity $\vec{v}$; σ is the elastic scattering cross section. Neglecting inelastic collisions and heating, the EVDF is determined by the kinetic equation,

$$v_x\left.\frac{\partial f}{\partial x}\right|_\varepsilon=n_a\int(f'-f)v\frac{d\sigma}{d\Omega}d\Omega.$$

We seek a solution of this equation for the EVDF in the loss cone. The EVDF outside the loss cone is much larger than

inside the loss cone, therefore $f' \gg f$ and can be neglected in the collision integral on the right-hand side of the equation. Then, direct integration of the equation gives the EVDF as an integral over time of flight of the scattering rate from outside of the loss cone to the loss cone,[15]

$$f_{lc}(x,\mathbf{v}) = n_a \int_x^L dx' \frac{1}{v_x} \int_0^{\pi/2} v f'(x',\mathbf{v}') \frac{d\sigma}{d\Omega} d\Omega. \quad (1)$$

For an isotropic EVDF the integration over angles is straightforward and $f_{lc}(x,\mathbf{v}) = n_a \int_x^L dx' v\sigma f(x',v)/v_x$. Therefore, the EVDF in the loss cone is smaller by a factor of order $H\sigma n_a = H/\lambda_c$ compared with the EVDF outside the loss cone. For an anisotropic EVDF the integration cannot be carried out analytically. However, the ratio of the EVDF in the loss cone to the EVDF outside the loss cone is also proportional to H/λ_c with some correction factor of order unity, which is necessary to account for the EVDF anisotropy.

III. PARTICLE FLUXES TO THE WALLS IN HALL THRUSTER CHANNEL

A. Strong reduction of the electron fluxes to the walls due to the depleted loss cone compared with predictions of fluid theories

As shown in the previous section the electron flux to the wall in the limit of the large electron mean free path $\lambda_c \gg H$ is reduced by a factor of order H/λ_c compared with the calculation assuming an EVDF with a filled loss cone. For typical thruster conditions $H/\lambda_c \sim 1/100$ and the reduction is considerable. Making use of Eq. (1) the electron flux to the wall can be written as

$$\Gamma_e \simeq \frac{H}{8\lambda_c} n_e \sqrt{\frac{8T_{ez}}{\pi m}} \exp\left(-\frac{\Phi}{T_{ez}}\right). \quad (2)$$

Here, n_e is the plasma density in the center; see, e.g., Ref. 28 for details. For a Maxwellian isotropic EVDF the flux to the wall is equal to $1/4 n_w \sqrt{8T_e/\pi m}$, where n_w is the density at the wall, which relates to the central density through the Boltzmann relationship $n_w = n_e \exp(-e\Phi/T_e)$. Equation (2) has two major differences from the fluid model: the electron temperature T_{ez} enters the equation, and there is an additional small factor, $H/2\lambda_c$, which accounts for strong reduction of the electron flux due to the depleted loss cone. The exact coefficient 1/2 was chosen to fit best the simulation results (compare lines 19 with 17 in Table I).

In Eq. (2), we used the fact that for most of our calculations the temperature in the z direction is larger than the temperature in the x direction. Electrons scattered into the loss cone (i.e., lost to the walls) have a total energy of more than $e\Phi$ and mostly originate from large pitch angle scattering. Therefore, the fraction of these electrons and their velocity are determined by the electron temperature in the direction of the external electric field rather than in the direction to the walls. This explains why T_{ez} appears in Eq. (2) instead of T_{ex}.

B. Penetration coefficients of secondary electron emission beams

The secondary electrons emitted from the opposite walls are accelerated in the near-wall sheaths towards the plasma and form counterstreaming beams. For a quasistationary symmetric plasma, the wall potentials at the opposite walls are the same. When the beam electrons penetrate through the plasma bulk, they may gain enough energy (due to the $E \times B$ motion) to induce the SEE from the opposite wall. References 10, 11, and 18 introduced a phenomenological coefficient (α) to describe the penetration of the SEE beam from one wall to the opposite wall. The scattering of the SEE beams can occur due to collisions with atoms or bulk plasma electrons. However, the probability for such scattering to occur is small (about a few percent) because the electron mean free path is very large for typical thruster conditions. Another mechanism of scattering involves the high-frequency electric-field oscillations with a period shorter or comparable with electron time of flight from one wall to another. A possible candidate of high-frequency electric-field oscillations is the two-stream instability between the SEE beam and bulk electrons. Such instability excites the plasma oscillations with the frequency close to the electron plasma frequency. The necessary condition for this instability is a nonmonotonic 1D EVDF $f_x(v_x) = \int_0^\infty f(v_x, w_\perp) dw_\perp$. The 1D EVDF can become nonmonotonic due to presence of a very large number of SEE electrons. PIC simulations confirm such theoretical predictions; see Refs. 10 and 29 for details.

The two-stream instability results in the energy transfer from the SEE beam to bulk electrons, therefore some SEE beam electrons cannot leave the plasma because their w_x energy becomes smaller than the potential energy at the wall, $w_x < e\Phi$. This leads to accumulation of loosely trapped in plasma potential or "weakly confined" former SEE beam electrons. However, after a certain time these electrons can acquire energy from "fresh" SEE beam electrons and leave the plasma. Figure 5 shows the temporal evolution of the SEE fluxes. About 20% of the SEE beam does not reach the opposite wall. However, the reduction of flux is totally compensated by the flux of weakly confined electrons. In PIC codes this reduction may also be attributed to the finite number of particles per computational grid cell and the associated electric-field noise.

To summarize: (i) The effective penetration coefficient should be equal to unity, i.e., all SEE electrons from one wall eventually reach the opposite wall, and (ii) the emitted electron flux is balanced by the sum of fluxes due to the beam and the weakly confined (former secondary) plasma electrons. In other words, the contribution of secondary electrons to the total current balance at the ceramic channel walls is canceled. This is seemingly similar to the plasma-wall interaction without SEE from the walls. However, according to the present model, the ion current to the wall is balanced by the flux of bulk electrons scattered into the loss cone, which is much smaller than the electron flux calculated in the fluid theories. Results of numerical simulations confirm this assumption (compare curves 1 and 2 in Fig. 5).

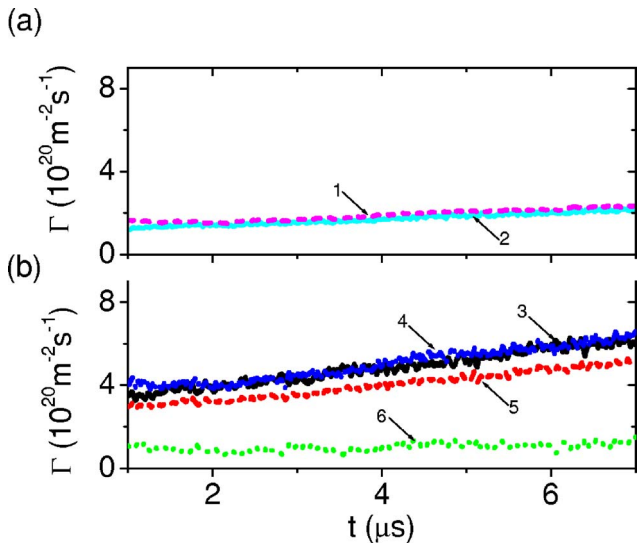

FIG. 5. (Color online) Temporal dependences of wall fluxes obtained in PIC simulation (case 1 of Table I). (a) Ion flux (1, magenta, dashed) and collision-ejected electron flux (2, cyan, solid) at the right wall, $x=H$. (b) Secondary electron beam emitted at the left wall $x=0$ (3, black, solid), secondary electron beam registered at $x=H$ (5, red, dashed), flux of weakly confined electrons at $x=H$ (6, green, dotted), sum of fluxes of the beam and of the weakly confined electrons at $x=H$ (4, blue, short-dashed).

C. Analytical estimate of the wall potential and collision-ejected electron flux

The ion flux can be estimated from the Bohm criterion and the fact that for a planar geometry the plasma density approximately decreases twice from the plasma center to the plasma sheath boundary in a collisionless case (when ion mean free path is large compared with the channel); see, for example, Ref. 28,

$$\Gamma_i = \tfrac{1}{2} n_e \sqrt{T_{ex}/M}. \tag{3}$$

Table I compares results of calculations for the electron, Γ_e, and ion, Γ_i, fluxes based on analytical formulas of Eqs. (2) and (3), respectively, with simulation data (compare lines 18 and 19 with 17). An agreement between analytical and numerical results is surprisingly good, given the fact that the analytical model uses approximate estimates rather than exact calculations.

Because the SEE beams do not contribute to the current balance at the walls, the ambipolarity criterion implies that the ion wall flux is compensated by the collision-ejected electron flux $\Gamma_i=\Gamma_e$. Under such conditions, the plasma potential at the center with respect to the wall (i.e., the potential drop in the sheath and presheath) can be determined from Eqs. (2) and (3), and reads

$$\Phi = \frac{T_{ez}}{e} \ln\left(\frac{H}{\lambda_c} \sqrt{\frac{T_{ez}}{T_{ex}}} \sqrt{\frac{M}{2\pi m}} \right). \tag{4}$$

For the conditions of Fig. 1, the contribution from the sheath potential gives 5.3, the potential drop in the plasma gives 0.70, and the reduction due to empty loss cone gives −5.1, totaling the value of the wall potential being of order T_{ez}/e,

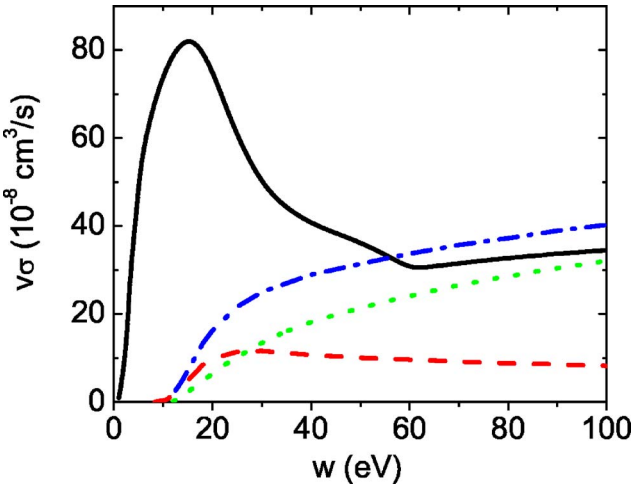

FIG. 6. (Color online) The frequency scaling of the electron impact collisions in xenon. (Solid black line) the elastic scattering; (dashed red line) excitation; (dotted green line) ionization; (dot-dashed line) the sum of ionization and excitation cross sections.

$$\Phi \approx \frac{T_{ez}}{e}\left[\sqrt{\frac{M}{2\pi m}} + \ln 2 - \ln\left(\frac{2\lambda_c}{H} \sqrt{\frac{T_{ex}}{T_{ez}}} \right) \right]$$
$$= \frac{T_{ez}}{e}(5.3 + 0.7 - 5.1) \approx \frac{T_{ez}}{e}. \tag{5}$$

The first term is the sheath potential, the second is due to the potential drop in the plasma, and the last term accounts for reduction of the electron flux due loss cone. Note a big contribution of the term describing the reduction of the electron flux due to the loss-cone effects, not described in the current fluid and kinetic theories.

Let us emphasize here that the result of Eq. (5) is only superficially similar to the result obtained by the fluid theory for the sheath potential drop in the space-charge-limited regime of the sheath.[2–5] The physical meaning of Eq. (5) is fundamentally different because the SEE's contribution to the flux balance is self-canceled and, therefore, the plasma potential with respect to the wall does not depend on the SEE.

IV. REASON FOR ANISOTROPIC ELECTRON VELOCITY DISTRIBUTION FUNCTION

In a typical gas discharge, the EVDF is isotropic, i.e., it is a function of a single variable, the electron speed, $f(v)$. The reason for isotropic EVDF is that the energy relaxation time for an electron is longer than the scattering time due to collisions, or the energy relaxation frequency is smaller than the electron-neutral elastic scattering collision frequency,[30]

$$\nu_{\text{loss}} \ll \nu_{en}. \tag{6}$$

Here, $\nu_{\text{loss}}=\nu_{\text{wall}}+\nu_{exc}+\nu_{iz}$ is the energy relaxation frequency determined by the wall losses, excitation, and ionization processes. As evident from Fig. 6, if the electron kinetic energy is above 40 eV, the total inelastic collision frequency due to excitation and ionization becomes comparable with the elastic scattering collision frequency $(\nu_{exc}+\nu_{iz}) > \nu_{en}/2$ for xe-

non. As a result, inequality (6) becomes weaker leading to the EVDF anisotropy.

Moreover, for electrons with energy larger than the confinement threshold, $w > e\Phi$, wall losses are the fastest energy loss mechanism and the characteristic energy relaxation frequency becomes the frequency of scattering into the loss cone, which equals to the collision frequency of elastic scattering times the probability to be scattered into the loss cone.[13] This probability is determined by the ratio of the loss-cone angle, Ω, to the entire sphere, which gives

$$\nu_{\text{wall}} \approx \nu_{en}\Omega/4\pi. \tag{7}$$

As shown in Sec. II, accounting for the two walls, the loss cone for electron energies w is

$$\Omega = 4\pi\frac{w - e\Phi}{w}. \tag{8}$$

Substituting Eq. (7) into Eq. (8) yields the effective loss frequency due to scattering to the loss cone and subsequent loss to the walls,

$$\nu_{\text{wall}} \approx \nu_{en}\frac{w - e\Phi}{w}\Theta(w - e\Phi). \tag{9}$$

Here, we added the Heaviside function to indicate that the wall losses occur only for electrons with energies above the confinement threshold, $w > e\Phi$.

Summing all energy losses into the total energy relaxation frequency, the criterion for the EVDF anisotropy can be written as

$$\nu_{en}\frac{w - e\Phi}{w}\Theta(w - e\Phi) + \nu_{exc} + \nu_{iz} > \frac{1}{2}\nu_{en}. \tag{10}$$

For $w > 2e\Phi$ the loss cone is wide, which gives the large effective energy relaxation frequency, and anisotropy should be expected for this energy range.

In summary, an electron undergoes just few scattering collisions before it is lost to the walls or loses its energy due to excitation or ionization. Because the number of collisions is small, the EVDF does not relax to an isotropic EVDF. The farther estimates of these effects are given in the next section.

V. ANALYTICAL ESTIMATES FOR ELECTRON TEMPERATURES IN HALL THRUSTER CHANNEL

A. Analytical estimate of the electron temperature in the direction parallel to walls of the Hall thruster channel, T_{ez}

Figures 2 and 3 demonstrate that the EVDF can be described as a Gaussian function with a temperature T_{ez} in the direction parallel to walls of the Hall thruster channel. This fact may be somewhat incidental and may change for very different thruster parameters. Nevertheless, for practically all our simulations the EVDF $f(v_z)$ was very close to a Gaussian (Maxwellian) in a very large range of the electric and magnetic fields; some possible explanations are given below. This is why T_{ez} is defined here as the energy value decreasing e times the EVDF over z velocity and assumed to be the same (constant) for different energy ranges. The flux of energetic electrons to the walls is determined by this temperature and wall potential. As evident from Fig. 6, for the electrons with kinetic energies less than 40 eV, it is more probable to escape to the walls than to lose their energy on ionization and excitation, $\nu_w > (\nu_{exc} + \nu_{iz})$. Therefore, the electron temperature T_z can be roughly estimated from the balance of the electron heating and wall energy losses for these fast electrons. A similar balance approach was used in Ref. 16 to estimate the electron-wall collision frequency for the measured electron temperature and known plasma conditions, where the ionization and excitation losses are negligible compared to the electron energy losses at the walls. The Joule heating for electrons constituting the high-energy tail of the EVDF can be written as

$$J_{ezf}E_zH \approx \frac{\nu_{\text{turb}} + \nu_{en}}{\omega_c^2 m}e^2E_z^2n_{ef}H, \tag{11}$$

where n_{ef} is the effective density of electrons with energy larger than the confinement threshold, $w > e\Phi$, and J_{ezf} is the current carried by fast electrons. The rate of the wall losses can be expressed as $Q_\varepsilon \approx \langle\nu_w\rangle n_{ef}T_{ez}H$. Here, $\langle\nu_w\rangle$ is the averaged wall loss frequency from Eq. (9), which is within 20% accuracy and can be approximated by $\langle\nu_w\rangle = \nu_{en}T_{ez}/(e\Phi + T_{ez})$. Thus the rate of the wall losses reads

$$Q_\varepsilon = \nu_{en}\frac{T_{ez}^2}{e\Phi + T_{ez}}n_{ef}H. \tag{12}$$

Equations (4), (11), and (12) allow to determine the electron temperature, T_{ez}, and the plasma potential. By equating Eqs. (11) and (12), and using Eq. (4), the approximate expression for the electron temperature in the direction of the electric field is

$$T_{ez} \approx k\left(1 + \frac{\nu_{\text{turb}}}{\nu_{en}}\right)m_e\left(\frac{E}{B}\right)^2\left(1 + \ln\left(\frac{H}{\lambda_c}\sqrt{\frac{T_{ez}}{T_{ex}}\frac{M_i}{2\pi m_e}}\right)\right), \tag{13}$$

where k is the correction coefficient, which can be obtained by a comparison of the approximate temperature estimations with the *exact* result of PIC simulations. The comparison of Eq. (13) with simulation data is shown in Table I (compare lines 22 and 9). An agreement is again satisfactory given the fact that approximate calculations were performed only as an order of magnitude estimate. The correction coefficient k is varied between 1.4 and about 2. For the thruster conditions in Figs. 2 and 3, Eq. (13) can be simplified using Eq. (5): $T_{ez} \approx 2k(1 + \nu_{\text{turb}}/\nu_{en})m_e(E/B)^2$. The correction factor k can be attributed to the fact that the EVDF $f(v_z)$ is not exactly a Maxwellian with a constant slope in semilogarithmic plot; whereas Eq. (13) approximates the electron temperature in the EVDF tail, rather than in the bulk, as given in Table. I.

Note that Eq. (13) can be also derived making use of the average kinetic equation, similar to the analysis performed in Ref. 19. The electron heating is described in such an approach as the energy diffusion process towards higher energies with the energy diffusion coefficient $D_\varepsilon \approx 1/2(\nu_{en} + \nu_{\text{turb}})(\Delta\varepsilon)^2$, which is the product of the effective scattering frequency $(\nu_{en} + \nu_{\text{turb}})$ and the energy step, $\Delta\varepsilon = eE\rho_c$, ac-

quired by an electron from the electric field during a spatial step in the z direction on one electron cyclotron radius $\rho_c = v_\perp/\omega_c$. Diffusion process is balanced by the losses with the frequency ν_w, which gives for the electron temperature estimate

$$T_{ez} \sim 2\sqrt{D_\varepsilon/\nu_w} = \sqrt{\frac{2(\nu_{en}+\nu_{\text{turb}})}{\nu_w}}\Delta\varepsilon. \tag{14}$$

Substituting expressions for $\Delta\varepsilon$ and ν_w into Eq. (14) gives the same Eq. (13). Note that because the wall loss frequency is comparable to the elastic scattering frequency and the turbulent collision frequency is not much larger than the elastic scattering frequency, the factor $\sqrt{2(\nu_{en}+\nu_{\text{turb}})/\nu_w}$ is just a few times. It means that electron heating occurs on distances of the order of few cyclotron radii and the energy relaxation length is also small, as has been discussed above at the beginning of Sec. II.

B. Analytical estimate of the electron temperature in the direction perpendicular to walls of the Hall thruster channel, T_{ex}

The estimate for the electron temperature is the most difficult one. Electrons are heated in the z direction and scatter due to elastic collisions in the x direction. The electron temperature is determined by the electron energy where electrons start to considerably lose their energy, which corresponds to energy, $w = e\Phi + T_{ez}$ in the z direction. Under conditions of a Hall thruster discharge, the confinement threshold $e\Phi$ is smaller or comparable with the electron temperature in the z direction, $e\Phi \sim T_{ez}$; see Eq. (5) and Table I (compare lines 7 and 9). This means that the loss cone

$$\Omega = 4\pi\frac{T_{ez}}{e\Phi + T_{ez}}$$

is wide for these energies, and the average frequency of electron losses to the walls $\langle\nu_w\rangle = \nu_{en}T_{ez}/(e\Phi+T_{ez})$ is comparable to the elastic scattering frequency, $\langle\nu_w\rangle \sim \nu_{en}$. Electrons do not have enough time to scatter (isotropize) energy acquired from the electric field in the z direction, and the EVDF becomes anisotropic. Moreover, the transformation of energy from the y,z directions to the x direction occurs due to scattering within of the outside of the loss cone, $(1-\Omega/4\pi)$ (if electrons scatter inside the loss cone they are quickly lost). The ratio of temperatures can be estimated as $T_{ex} \sim T_{ez}(1-\Omega/4\pi)$. Then, substituting the equation for the loss cone gives

$$T_{ex} \approx \frac{e\Phi}{e\Phi + T_{ez}}T_{ez}, \tag{15}$$

where the ratio $e\Phi/T_{ez}$ can be obtained from Eq. (4). There is a satisfactory agreement between the approximate results obtained from Eq. (15) with the exact results of PIC simulations (Table I, lines 21 and 8). Note that if $e\Phi \gg T_{ez}$, the loss cone is small $(1-\Omega/4\pi) \approx 1$ and $T_{ex}/T_{ez} \to 1$, the EVDF becomes isotropic. In the opposite limit $e\Phi < T_{ez}$, the loss cone is large, $\Delta\Omega \to 4\pi$, and according to Eq. (15), $T_{ex}/T_{ez} < 1$, the EVDF is anisotropic (see Table I, lines 7–9).

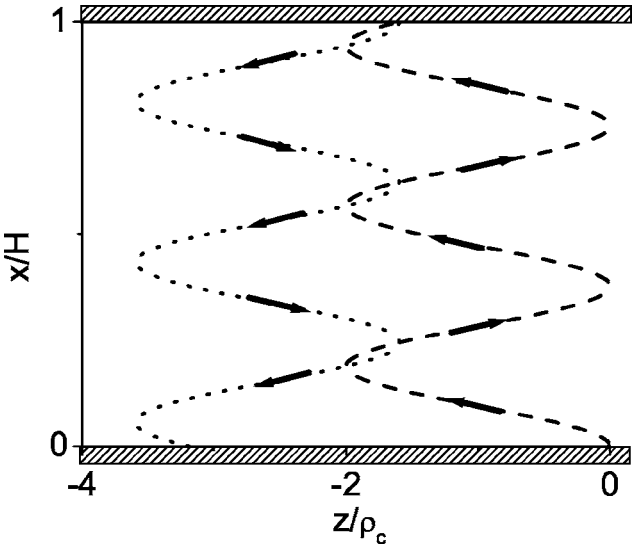

FIG. 7. Schematics of SEE electron trajectory and SEE contribution to the total current.

VI. ELECTRON CROSS-FIELD CURRENT INDUCED BY SECONDARY ELECTRON EMISSION BEAMS

The SEE beams can carry a considerable fraction of the total current (Table I, lines 15 and 16). The velocity in the direction of the current of the secondary electrons in the crossed electric and magnetic fields is given by

$$u_{bz}(x) = -\frac{E_z}{B_x}\sin\left(\omega_c\int_0^x dx\frac{1}{u_{bx}(x)}\right), \tag{16}$$

where $u_{bz}(x)$ and $u_{bx}(x)$ are the beam velocity components; see Fig. 7. The electric current density along the z direction created by the electrons of a SEE beam and averaged over the channel width is

$$J_{bz} = -\frac{e}{H}\int_0^H dx n_b(x)u_{bz}(x), \tag{17}$$

where

$$n_b(x) = \frac{\Gamma_b}{u_{bx}(x)} = \frac{\gamma_p\Gamma_i}{(1-\gamma_b)u_{bx}(x)} \tag{18}$$

is the beam density, Γ_b and Γ_i are the beam and the ion fluxes towards the wall, and γ_b and γ_p are the partial emission coefficients due to the electrons of the beam and the plasma bulk, respectively. Here, we used the expression for the beam flux from Refs. 10–12. Assuming for simplicity that the beam velocity normal to the walls is constant, $u_{bx}(x) \approx \bar{u}_{bx} = \sqrt{2e\Phi/m}$, and substituting $u_{bz}(x)$ from Eq. (16) and $n_b(x)$ from Eq. (18) into Eq. (17) with the ion flux (3), one obtains

$$J_{bz} \approx \frac{m}{H}\frac{\gamma_p}{1-\gamma_b}\frac{1}{2}n_e\sqrt{\frac{T_{ex}}{M}}\frac{E_z}{B_x^2}\int_0^{\varphi_H} d\varphi\sin\varphi, \tag{19}$$

where $\varphi_H \approx H\omega_c/\bar{u}_{bx}$ is the maximal phase of cyclotron rotation of the beam. PIC simulations with typical Hall thruster parameters show that usually $\varphi_H \approx 2\pi n + 3\pi/2$, where $n = 1,2,\ldots$. Then the integral in (19) is equal to unity, and the

electric current density due to the SEE beams emitted from both walls is

$$J_{bz} \approx \frac{m}{H}\frac{\gamma_p}{1-\gamma_b} n_e \sqrt{\frac{T_{ex}}{M}}\frac{E_z}{B_x^2}. \tag{20}$$

Note that the parameters of γ_p, γ_b depend on the electron temperature, wall potential, and electric field.

This current can significantly contribute to the total conductivity and may explain the influence of wall material on thruster operation observed in experiments,[1,2,17] as well as the influence of the channel width on the electron temperature.[31] This estimate is similar to Morozov's prediction of the near-wall conductivity[32–34] but calculated self-consistently.

The physical explanation for the current in Eq. (20) is as follows. The SEE electron during one pass from the wall to the opposite wall moves in the z direction by the distance of order $\rho_c = v_\perp/\omega_c$, where $v_\perp = u_d = E_z/B_x$. Then, the average velocity in the z direction is $\langle u_z\rangle \sim \rho_c/(H/\bar{u}_{bx}) = u_d u_{bx}/H\omega_c$; see Fig. 6. The expression for the current density $J_{bz} = en_b\langle u_z\rangle$ corresponds to the exact calculation in Eq. (20). Table I contains the values of the electric current density due to the SEE beams obtained in simulations (line 16) and analytically making use of Eq. (20) (line 24). There is a fairly good agreement between the numerical and analytical values. Note that for simulation case 3 in Table I, the SEE beams create the major part of the current.

VII. CONCLUSIONS

We derived simplified analytical formulas for averaged kinetic plasma parameters of a Hall thruster. The system consists of equations for electron flux to the wall,

$$\Gamma_e \simeq \frac{H}{8\lambda_c} n_e \sqrt{\frac{8T_{ez}}{\pi m}} \exp\left(-\frac{\Phi}{T_{ez}}\right),$$

for the ion flux to the walls,

$$\Gamma_i = \tfrac{1}{2} n_e \sqrt{T_{ex}/M},$$

flux balance assuming that SEE fluxes completely compensate each other,

$$\Gamma_i = \Gamma_e;$$

the balance of fluxes yields formulas for the wall potential

$$\Phi = \frac{T_{ez}}{e}\ln\left(\frac{H}{\lambda_c}\sqrt{\frac{T_{ez}}{T_{ex}}}\sqrt{\frac{M}{2\pi m}}\right).$$

The electron temperature in the direction parallel to the walls can be obtained from the energy balance equation for fast electrons, which gives

$$T_{ez} \approx k\left(1+\frac{\nu_{\text{turb}}}{\nu_{en}}\right) m_e\left(\frac{E}{B}\right)^2\left(1+\ln\left(\frac{H}{\lambda_c}\sqrt{\frac{T_{ez}}{T_{ex}}}\frac{M_i}{2\pi m_e}\right)\right),$$

where fitting parameter k varies between 1.4 and 2. The electron temperature in the direction perpendicular to the walls can be obtained from analysis of loss cone, which gives

$$T_{ex} \approx \frac{e\Phi}{e\Phi + T_{ez}} T_{ez}.$$

Finally, the contribution of SEE electrons to the total current reads

$$J_{bz} \approx \frac{m}{H}\frac{\gamma_p}{1-\gamma_b} n_e \sqrt{\frac{T_{ex}}{M}}\frac{E_z}{B_x^2},$$

where γ_b and γ_p are the partial emission coefficients due to the electrons of the beam and the plasma bulk, respectively.

The plasma potential, the wall electron flux, and the electron temperatures calculated making use of these formulas agree well with the values obtained in particle-in cell simulations. The SEE effect on power losses in a thruster discharge is shown to be quite different from what was predicted by previous fluid and kinetic studies. Kinetic calculation gives the values of the electron flux of a few orders of magnitude smaller than the values obtained using the fluid approach. The difference is attributed to the presence of a large depleted loss cone in the electron velocity distribution function. The EVDF in the loss cone is determined by elastic scattering of electrons due to collisions with atoms and Coulomb collisions. Our results suggest that even in the presence of a strong SEE from the walls, a contribution of the wall energy losses to the electron energy balance is much smaller than predicted by fluid theories and is proportional to the elastic scattering of electrons on collisions with atoms and ions and not inversely proportional to the electron time of flight to the walls, as is commonly assumed. It means that the wall flux is proportional to the gas density and is independent on the channel width (as long as $H \ll \lambda_c$). This is very different from plasmas with the isotropic electron EVDF, including Maxwellian and non-Maxwellian EVDFs.

Another important result of these kinetic studies is that the SEE contribution to the current balance at the walls is self-canceled and, therefore, the plasma potential with respect to the wall and the electron energy losses on the walls are almost insensitive to the SEE. Secondary electrons emitted from the walls form two counterstreaming beams. The effective coefficient for penetration of the SEE beams from one wall to the opposite wall is equal to unity. One may assume the complete penetration of the emitted electrons because the beam electrons, which lose energy due to the two-stream instability and cannot leave the plasma in one pass between the channel walls, will eventually gain energy and escape the plasma. The SEE beams may carry a considerable portion of the cross-field electron current due to their cycloid trajectory in the $E\times B$ field. This effect should depend on SEE properties of the channel wall material.

Finally, the results of these theoretical studies may explain the influence of wall material on the thruster operation and plasma parameters observed in experiments,[1,2,17] as well as influence of the channel width on the electron temperature[31] by the enhancement of the electron conductivity due to contribution of the SEE electrons, rather than the enhancement of the energy losses to the walls. This conclusion is in agreement with the analysis of experimental data in

Ref. 16. Future studies should be focused on generalization of this model to the two-dimensional geometry.

ACKNOWLEDGMENTS

This research was partially supported by the Air Force Office of Scientific Research through the AF STTR Program and the U.S. Department of Energy Office of Fusion Energy Sciences.

[1] Y. Raitses, J. Ashkenazy, G. Appelbaum, and M. Guelman, *Proceedings of the 25th International Electric Propulsion Conference* (Electric Rocket Propulsion Society, Cleveland, OH, 1997), IEPC Paper No. 97-056.
[2] S. Barral, K. Makowski, Z. Peradzýnski, N. Gaskon, and M. Dudeck, Phys. Plasmas **10**, 4137 (2003).
[3] E. Ahedo and D. Escobar, J. Appl. Phys. **96**, 983 (2004).
[4] G. D. Hobbs and J. A. Wesson, Plasma Phys. **9**, 85 (1967).
[5] V. A. Rozhansky and L. D. Tsendin, *Transport Phenomena in Partially Ionized Plasma* (Taylor & Francis, London, 2001).
[6] E. Ahedo, J. M. Gallardo, and M. Martinez-Sanchez, Phys. Plasmas **10**, 3397 (2003).
[7] M. Keidar, I. Boyd, and I. I. Beilis, Phys. Plasmas **8**, 5315 (2001).
[8] N. Meeazan and M. Cappelli, Phys. Rev. E **66**, 036401 (2002).
[9] O. Batishchev and M. Martinez-Sanchez, *Proceedings of the 28th International Electric Propulsion Conference* (Electric Rocket Propulsion Society, Cleveland, OH, 2003), IEPC Paper No. 2003-188.
[10] D. Y. Sydorenko and A. I. Smolyakov, Bull. Am. Phys. Soc. **49**, 261 (2004).
[11] D. Sydorenko, A. Smolyakov, I. Kaganovich, and Y. Raitses, Phys. Plasmas **13**, 014501 (2006).
[12] D. Sydorenko, A. Smolyakov, I. Kaganovich, and Y. Raitses, IEEE Trans. Plasma Sci. **34**, 815 (2006).
[13] I. Kaganovich, *Proceedings of the 29th International Electric Propulsion Conference* (Electric Rocket Propulsion Society, Cleveland, OH, 2005), IEPC Paper No. 2005–096.
[14] L. D. Tsendin, Sov. Phys. JETP **39**, 805 (1974).
[15] I. Kaganovich, M. Misina, S. V. Berezhnoi, and R. Gijbels, Phys. Rev. E **61**, 1875 (2000).
[16] Y. Raitses, D. Staack, A. Smirnov, and N. J. Fisch, Phys. Plasmas **12**, 073507 (2005).
[17] Y. Raitses, D. Staack, A. Smirnov, and N. J. Fisch, Phys. Plasmas **13**, 014502 (2006).
[18] E. Ahedo and F. I. Parra, Phys. Plasmas **12**, 073503 (2005).
[19] I. D. Kaganovich and L. D. Tsendin, IEEE Trans. Plasma Sci. **20**, 66 (1992).
[20] D. Staack, Y. Raitses, and N. J. Fisch, Appl. Phys. Lett. **84**, 3028 (2004).
[21] J. M. Hagelaar, J. Bareilles, L. Garrigues, and J.-P. Boeuf, J. Appl. Phys. **91**, 5592 (2002).
[22] J. M. Fife, Ph.D. thesis, Massachusetts Institute of Technology, 1998.
[23] J. M. Haas and A. D. Gallimore, Phys. Plasmas **8**, 652 (2001).
[24] J. A. Linnell and A. D. Gallimore, Phys. Plasmas **13**, 103504 (2006).
[25] D. Gawron, S. Mazouffre, and C. Boniface, Plasma Sources Sci. Technol. **15**, 757 (2006).
[26] L. Garrigues, G. J. M. Hagelaar, J. Bareilles, C. Boniface, and J. P. Boeuf, Phys. Plasmas **10**, 4886 (2003).
[27] G. Guerrini, C. Michaut, M. Bacal, A. N. Vesselovzorov, and A. A. Pogorelov, Rev. Sci. Instrum. **69**, 804 (1998).
[28] I. D. Kaganovich, Phys. Plasmas **9**, 4788 (2002).
[29] D. Sydorenko, A. Smolyakov, I. Kaganovich, and Y. Raitses, Phys. Plasmas **14**, 013508 (2007).
[30] I. D. Kaganovich and L. D. Tsendin, IEEE Trans. Plasma Sci. **20**, 86 (1992).
[31] Y. Raitses, D. Staack, M. Keidar, and N. J. Fisch, Phys. Plasmas **12**, 057104 (2005).
[32] A. I. Morozov, Fiz. Plazmy **3**, 19 (1968).
[33] V. A. Kurochkina and A. P. Shubin, Sov. J. Plasma Phys. **17**, 806 (1991).
[34] A. A. Ivanov, A. A. Ivanov, Jr., and M. Bakal, Plasma Phys. Controlled Fusion **44**, 1463 (2002).